Implementation of a perturbation model for a dilute binary liquid and comparison of model mass diffusion coefficients with microgravity experiment results for liquid Pb 1 wt % Au

Paul J. Scott and Reginald W. Smith

Abstract: The estimation of mass diffusion coefficients, through Earth-bound experiments, remains difficult, due to the frequent occurrence of dominating convective flows resulting from gravity-driven density gradients caused by temperature and concentration gradients. To partly remedy this, a series of capillary mass diffusion experiments has been performed in microgravity on a number of different space platforms, sometimes performed on a microgravity isolation mount, to further reduce the platform operational noise referred to as "*g*-jitter". Theoretical comparisons are sought for the experimental observations. Two numerical models have been developed based on perturbation theory. We have used the Lado criteria for minimizing the difference in free energy between the multispecies liquid of interest and a reference hard-sphere liquid. The hard-sphere liquid is characterized by the rational function approximation of the partial radial distribution functions. The effective embedded atom like glue potential has been used to model the liquid of interest. This has necessitated introducing the mean coordination number as an additional parameter. Isothermal compressibility has been used to determine the mean coordination number. The initialization of the numerical solutions, and the extension of solutions over the experimental range of temperatures have been demonstrated for Pb 1 wt % Au. The model results have been used to estimate the mass diffusion coefficients by applying the Enskog equation to the reference hard-sphere liquid. For consideration of capillary experiments, a definition of total mass diffusion coefficient, D_{tot}, has been introduced to characterize reverse Kirkaldy simultaneous diffusion. The mixed diffusion coefficient estimate is in good agreement with the mixed diffusion coefficient estimated from the velocity correlation of molecular dynamic simulations. D_{tot} and D_{11} are in good agreement with the experimental results indicating that reverse Kirkaldy simultaneous diffusion has had an influence on the experiment. Good agreement between the mixed mass diffusion coefficient and the result from molecular dynamic simulation indicates the perturbation models can predict the mixed coefficient. These models may assist in the analysis of data from both Earth-bound and microgravity, mass diffusion experiments when the required embedded atom type potentials are available.

PACS Nos: 11.25.Db, 02.60.Nm, 66.10.cg, 61.25.Mv

Résumé : Il demeure difficile d'évaluer les coefficients de diffusion massique dans des expériences sur Terre, à cause des fréquents courants de convexion souvent dominants générés par des gradients de densités dus à la gravité et dont la source se trouve dans les gradients de température et de concentration. Pour remédier partiellement à ce problème, nous avons fait une série d'expériences de diffusion massique en capillaire en état de microgravité à bord de différentes plateformes spatiales, souvent sur un support d'isolation de microgravité afin de réduire encore plus le bruit opérationnel, appelé *fluctuation g*, sur les plateformes. Nous cherchons à comparer à des valeurs théoriques. Nous avons ici utilisé deux modèles numériques basés sur la théorie des perturbations. Nous avons utilisé le critère de Lado pour minimiser la différence d'énergie libre entre le liquide mixte d'intérêt et une sphère dure de liquide de référence. Le potentiel effectif de type adhésif pour l'atome incorporé sert à modéliser le liquide à l'étude. Nous avons dû introduire un nouveau paramètre de coordination moyenne. Nous utilisons la compressibilité isotherme pour fixer ce nombre de coordination. Nous avons débuté la simulation et avons étendu la solution à un domaine de température valable pour du Pb à 1 % de Au en poids. Les résultats du modèle ont été utilisés pour estimer les coefficients de diffusion en appliquant l'équation de Enskog à la sphère dure de liquide de référence. Pour étudier les expériences de diffusion capillaire, nous avons introduit un coefficient de diffusion massique totale, D_{tot}, afin de caractériser la diffusion simultanée inverse de Kirkaldy. Le coefficient de diffusion mixte estimé est en bon accord avec la valeur calculée par corrélation de vitesse en simulation dynamique moléculaire. D_{tot} et D_{11} sont en bon accord avec les résultats expérimentaux, indiquant que la diffusion inverse de Kirkaldy a eu une influence sur l'expérience. Le bon accord entre les coefficients mixtes de diffusion massique et les résultats de dynamique moléculaire indique que les modèles perturbatifs peuvent prédire les coefficients mixtes. Ces modèles pourront être utiles dans l'analyse des données d'expérience sur Terre et en microgravité dans l'espace, lorsque le potentiel effectif de type adhésif est connu.

[Traduit par la Rédaction]

Received 17 June 2009. Accepted 17 August 2009. Published on the NRC Research Press Web site at cjp.nrc.ca on 8 October 2009.

P.J. Scott[1] and R.W. Smith. Department of Mechanical and Materials Engineering, Queen's University, Kingston, ON K7L 3N6, Canada.

[1]Corresponding author (e-mail: pjs7@queensu.ca).

1. Introduction

The mass diffusion coefficient, and its relation to other system variables, is important as a source of fundamental knowledge and also because of its role in modeling both the control and optimization of material processing systems. The coefficient is difficult to measure on Earth because diffusion is often masked by gravity-riven convective flow originating from thermally and solute concentration gradient-induced density gradients. A series of diffusion experiments were performed by Queen's University on the Russian Space Station MIR, by Smith [1], using the Canadian Space Agency Microgravity Isolation Mount, (MIM), to further reduce the effects of environmental and operational sources of vibration referred to as "*g*-jitter", now over a decade later, these remain the only *g*-jitter free diffusion results available for analysis. The experimental results obtained for the Pb 1% wt Au alloy, had been compared with velocity correlation estimates from molecular dynamic simulation and the Enskog hard-sphere-corrected estimates using the radial distribution function provided by the molecular dynamic simulation in Scott et al. [2]. Three methods are described in Scott et al. [3] for using the Enskog equation [4, 5] to estimate mass diffusion coefficients of a dilute binary liquid from a reference hard-sphere liquid that is chosen to approximate combinations of static structure factor and isothermal compressibility data of the solvent. One of these methods assumes equal solvent and solute radii and satisfies an isothermal compressibility constraint. The resulting mass diffusion coefficient, denoted by D^{B} in Scott et al. [3] and here denoted by MB makes good agreement with several of the mass diffusion coefficient estimated here, and is reproduced in some figures for comparison. A fourth similar method is described in Scott et al. [6]. These four methods use the rational function approximation of the partial radial distribution functions, pRDF, of the hard-sphere liquid developed by Yuste et al. [7, 8]. Here, another theoretical comparison is sought that does not use velocity correlation estimates or molecular dynamic simulations. Rather, the Enskog equation is applied to a hard-sphere reference liquid and the rational function approximation of the pRDF is used. However the hard-sphere reference liquid is determined by a formal numerical procedure devised from perturbation theory. In the numerical procedure, embedded atom-like potentials [9, 10], which have proved to be quite effective in describing liquid-metal alloys, were used. Since perturbation theory is derived for two point potentials, while embedded atom-like potentials take into account all the neighbouring atoms within a specified radius, an effective embedded atom-like two-point potential is required. This necessitates introducing a mean coordination number. Experimental data about the isothermal compressibility of the solvent has been used to give an additional constraint for determining the mean coordination number at different temperatures. The use of the isothermal compressibility data of the solvent limits the method to dilute binary liquids. However, if isothermal compressibility data are available for the binary liquid the method should apply at higher solute concentrations. The result is a self-contained estimate of the mass diffusion coefficients based on first solving a system of nonlinear integral equations. Two such systems and have been considered: one system, **Model 2**, with equal hard-sphere solvent and solute radii and one system, **Model 1**, with unequal hard-sphere solvent and solute radii. Their precise characterization is given in Subsect. 2.6. Like any systems of nonlinear equations, searching for initial solutions is a nontrivial task and has been described here for both systems since similar searches should succeed for other binary liquids for which embedded atom-like potentials and isothermal compressibility data are available. In addition, the existence of only a small number of isolated solutions has been demonstrated, two for each system.

The combination of the perturbation criteria used here with effective embedded atom-like potentials , which introduces a mean coordination number, the rational function approximation for the pRDF of the hard-sphere reference liquid, and use of experimental isothermal compressibility data to determine the mean coordination number, is novel. Figure 15 indicates that the model mixed diffusion coefficient (notation explained in text) D_{12}^{U} makes good agreement with the velocity autocorrelation estimate "MD" obtained from molecular dynamic simulation described in ref 2. Model diffusion coefficients D^{S4}, D_{11}^{U}, and D_{tot}^{U} are almost identical with estimate MB described in ref. 3, and all four estimates make good agreement with the experimental data in Smith [1]. This last observation suggests that the capillary experiment is subjected to reverse Kirkaldy diffusion of the solvent, and that the mixed diffusion coefficient is not directly measurable, but must be inferred by application of models for which D_{tot}^{U} makes good agreement with the experimental observation.

Section 2 briefly discusses the perturbation approach used here with the precise description of **Model 1** and **Model 2** given in Subsect. 2.6, discusses the general numerical details of the implementation, describes the initialization process for both models, the solutions, and the resulting estimates of the mass diffusion coefficients are exhibited and compared with experimental results from Smith [1]. The paper ends with conclusions Sect 8.

2. Theory

Starting in the 1970s, a completely self-contained procedure for estimating the properties of a liquid of interest from the corresponding properties of a reference liquid was developed based on minimizing the integral functional expressing the difference or perturbation in free energy between the liquid of interest and a reference liquid. When the reference is a hard-sphere liquid, many of its properties are well known. For example, the Enskog equation [4, 5] can be applied to the hard-sphere reference liquid to estimate or infer the diffusion coefficients of the liquid of interest and several recent effective approximations are available for the hard-sphere liquid pRDF [7, 8]. There has been recent interest in applying perturbation methods to liquid metal alloys [11–13].

For liquids consisting of only one type of atom the basis of the perturbation model is to consider, at fixed temperature and volume, or density, the application with increasing parameter λ, of a perturbed interatomic potential

$$v = v^{o} + \lambda w$$

such that, at $\lambda = 0$, the potential v^{o} is that of the reference liquid, usually a hard-sphere liquid, and when $\lambda = 1$, the po-

tential $v = v^o + w$, is that of the liquid of interest. Throughout, it is assumed that v^o and w are additive potentials, so the total potential energy is the sum of the potential between pairs of atoms. While studying equations of state for fluids, Zwanzig [14] developed the high-temperature expansion for free energy [15] during which he showed the following inequality:

$$\frac{F}{k_B TN} \leq \frac{F^o}{k_B TN} + \omega_1 \tag{1}$$

where F is the free energy of the liquid of interest, F^o is the free energy of the reference liquid, N is the number of atoms in each liquid, and k_B is Boltzmann's constant. For a reference liquid consisting of a uniform liquid with constant atom number density ρ, and radial distribution function g [15], ω_1 has the form

$$\omega_1 = \frac{2\pi\rho}{k_B T}\int_0^\infty [v(r) - v^o(r)]g(r)r^2\,\mathrm{d}r \tag{2}$$

Equations (1) and (2) can also be determined using the Gibbs–Bolgoliubov inequalities [15] that ensure the perturbation process described above leads to a unique thermodynamic system when the free energy F is minimized. Since the liquid of interest is not understood in detail, minimization of F cannot be achieved directly. However, ω_1, given by (2), is expressed in terms of the radial distribution function of the reference liquid and when this can be approximated well, such as for the hard-sphere liquid, it is feasible to minimize ω_1 giving a lowest upper bound for the free energy of the liquid of interest. Minimization of the upper bound gives the best approximate model of the fluid of interest from which its properties such as mass diffusion can be approximated since ω_1 is expressible in terms of known properties of the liquid of interest and the reference liquid. This perturbation approach has been applied to study Leonard–Jones liquids, and the results compare well with results from molecular dynamic simulation [16]. The perturbation approach has also been the basis for several studies to determine the equation of state for liquids [17]. In addition a correction for the volume not accessible in a hard-sphere reference fluid is given in ref 18. In ref. 19, the correction was approximated by an integral term that could be added to (2). Although these refinements could be extended to the multi-species fluid, they were not used here.

A necessary (and sufficient condition for a unique solution when strict convexity applies), for a minimum of ω_1 given by (2) is the Lado criterion [20]

$$\int_0^\infty \left[\exp\left(-\frac{v(r)}{k_B T}\right) - \exp\left(-\frac{v^o(r)}{k_B T}\right)\right]\frac{\partial}{\partial\sigma}[g(r)]r^2\,\mathrm{d}r = 0 \tag{3}$$

where σ denotes the reference atom diameter, or some other length factor effecting $v^o(r)$, but assuming $v^o(r)$ does not depend on an energy scale [20]. This condition has the additional property that it provides consistency between the pressure and energy state equation [15] so the pressure computed by either state equation is the same and so the approximate model gives a thermodynamically consistent system. This leads to better results than other methods, such as the WAC "blip" function, (the expression in square brackets above) criterion [21]. The Lado criterion was extended to multi-species liquids [22]. For the multi-species case, let N_s denote the number of species, i, j, and k different species, x_i is the number concentration of species i at equilibrium, σ_i is the diameter of species i atoms in the reference liquid, $v_{ij}(r)$ is the interatomic potential between species i and i of the liquid of interest, $v_{ij}^o(r)$ is the interatomic potential between species i and j of the reference liquid and $g_{ij}(r)$ is the partial radial distribution function between species i and j of the reference fluid. For multi-species liquid, when no energy scales apply, the Lado criterion for each species k, from $l \leq k \leq N_s$ is

$$\sum_{i=1}^{N_s}\sum_{j=1}^{N_s} x_i x_j \int_0^\infty \left\{\exp\left[-\frac{v_{ij}(r)}{k_B T}\right] - \exp\left[-\frac{v_{ij}^o(r)}{k_B T}\right]\right\}\frac{\partial}{\partial\sigma_k}[g_{ij}(r)]r^2\,\mathrm{d}r = 0 \tag{4}$$

To implement these necessary conditions requires numerical specifications for both the interatomic potentials of the liquid of interest, $v_{ij}(r)$ and of the reference liquid, $v_{ij}^o(r)$, as well as approximations for the pRDF, $g_{ij}(r)$ of the reference liquid. These requirements are given in the following subsections.

2.1. Hard-sphere reference liquid interatomic potential specification

The hard-sphere liquid is most fully understood and is used here, as in most perturbation models, as the reference liquid. When N_s different species of atoms occur in the liquid, the hard-sphere liquid is completely determined by the hard-sphere diameters σ_i for $1 \leq I \leq N_s$. For atoms of two different species i and j, the diameter is given by the additive equation:

$$\sigma_{ij} = \frac{\sigma_i + \sigma_j}{2}$$

The hard-sphere interatomic potential is infinite up to diameter σ_{ij} and zero beyond that diameter. For the hard-sphere reference liquid, the Lado condition for optimality [22] given by (4), becomes, for each species k where $1 \leq k \leq N_s$

$$e_k \equiv \sum_{i=1}^{N_s}\sum_{j=1}^{N_s} x_i x_j \int_{\sigma_{ij}}^{v_{ij}^{\lim}(N_c)} \left[\exp\left(-\frac{v_{ij}(r, N_c)}{k_B T}\right) - 1\right] \times \frac{\partial}{\partial\sigma_k}[g_{ij}(r)]r^2\,\mathrm{d}r = 0 \tag{5}$$

where the interatomic potentials of the liquid of interest $v_{ij}(r, N_c)$ may depend upon some parameter N_c in addition to the interatomic distance r, and $v_{ij}^{\lim}(N_c)$ denotes the upper limit of the integral beyond which the two point interatomic potential is zero. The upper limit also depends upon the parameter N_c. When embedded atom-like potentials are introduced in Subsect. 2.3, N_c will have the physical interpretation of mean coordination number. Lastly, $g_{ij}(r)$ is given by an approximation of the pRDF of the reference liquid. In this way, the optimality criteria uses properties of both the liquid of interest and the reference liquid that are known or can be approximated.

2.2. Hard-sphere partial radial distribution function approximation

For the single species case [23] and multispecies case [24]

Fig. 1. Pb–Pb effective two point EAM potential [28, 31] with $N_c = 11.7$ and inverse power fit.

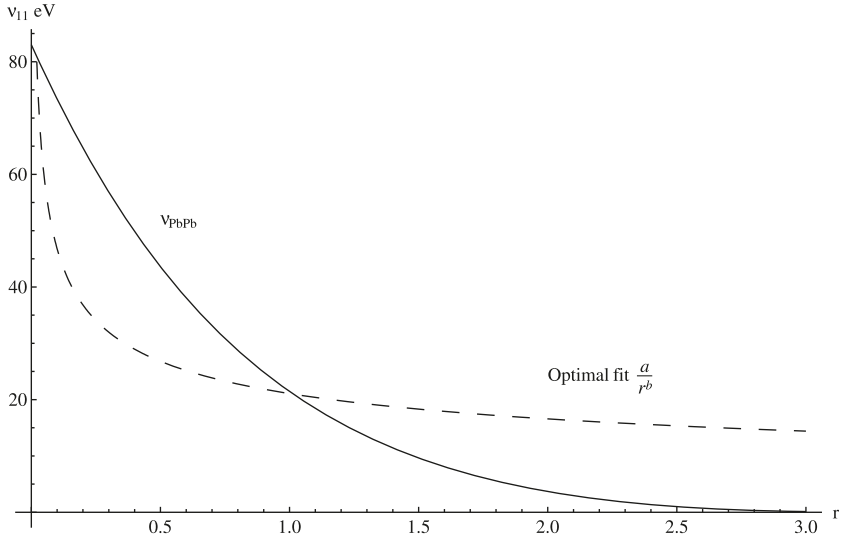

approximations of the hard-sphere pRDF are available by solution of the Percus–Yevick (PY) integral equations. A detailed derivation of the solution for the single species case is given in Hansen et al. [15]. However for the PY approximation, the pressure and isothermal compressibility equations of state are not consistent and so do not give a thermodynamic system. This problem was resolved using a rational function approximation, RFA, first for a single species fluid [7] then for a multispecies fluid [8]. The RFA is a fairly recent approximation and has proved to be just as good as some more recent and more complex approximations [25, 26]. *Mathematica* software is available for implementing the RFA approximation [27]. A brief introduction to the rational function approximation and a description of the input variables required to use the *Mathematica* implementation is given in ref. 3.

2.3. Interatomic potentials of liquid of interest Pb 1 wt % Au

The embedded atom method, EAM [9, 10], is an *n*-atom potential that includes the contribution from electrons surrounding the atoms within a prescribed radius of any given atom. It has been effective in describing pure liquid metals and liquid metal alloys. For this reason embedded atom like potentials were chosen here to give the interatomic potential of the liquid of interest. Fortunately, for the Pb 1 wt % Au liquid studied by Smith [1] embedded atom-like glue potentials are available for lead [28] and for gold [29]. An approximation used for the missing Pb–Au interatomic potential is given by eq. (6) of Landa et al. [30]. Hopefully EAM-like potentials are available for some of the other binary systems considered in Smith [1]. Effective two point potentials, necessary for the perturbation theory, were derived by applying the effective EAM, EEAM method described in Foiles [31].

The EEAM requires an estimate of the mean electron density in the neighbourhood of each atom. Because glue-type potentials were used, this requirement is replaced by the requirement of specifying the mean coordination number, N_c. For the EEAM, N_c is an additional parameter required to specify the interatomic potential as suggested in (5). For the fcc crystal the mean coordination number is $N_c = 12$, and for the liquid state lower values of N_c are expected. The interatomic potentials of the liquid of interest $v_{ij}(r, N_c)$ occur in the exponential term in the optimality criteria (5) for the radii of the corresponding hard-sphere reference liquid. For the numerical implementation, it is necessary to anticipate how $v_{ij}(r, N_c)$ will effect the numerical results. Figures 1–3 show the three effective two point potentials for the Pb 1 wt % Au liquid at $N_c = 11.7$. The units are length in angstroms, Å, and energy in electron volts, eV.

Notice from Figs. 1–3 that the potentials become zero beyond a finite radius $v_{ij}^{\lim}(N_c)$, which is different for each pair *ij*, and it was confirmed that it also varies with N_c. Because of the minus sign in the exponential, the potential at low values of *r* has greater effect on the integral. Once $v_{ij}(r, N_c) = 0$, the [ ] term occurring in each integral in (5) is zero.

The potentials are quite soft and remain finite at $r = 0$. The best fits by an inverse power law are also shown. Such approximations in earlier perturbation models reduce numerical calculation. However, since in this case, the fit is not very close, the potentials themselves were used in all calculations. It is also of interest that the gold potential v_{AuAu} in Fig. 3 is much higher than the lead potential v_{PbPb} in Fig. 1 and the mixed potential v_{PbAu} in Fig. 2 lies between the other two potentials.

Since the EEAM requires an additional parameter (for the glue type potentials, the mean coordinate number N_c) an additional constraint is required to determine this parameter. In the following two subsections, two constraints are described for determining N_c.

2.4. Isothermal compressibility constraint for N_c

The fluid density is required at each temperature. Experiments by Schwaneke et al. [32] indicate that the density, N/Å^3, of liquid Pb 1 wt % Au is well approximated by the linear relation

$$\rho = .03223 - .40538 \times 10^{-5}(T - 273) \qquad (6)$$

Values for the isothermal susceptibility, the limit as wavelength goes to infinity of the static structure factor, of liquid lead are found in refs. 33 and 34. From this the following

Fig. 2. Pb–Au effective two point EAM potential [30, 31] with N_c = 11.7 and inverse power fit.

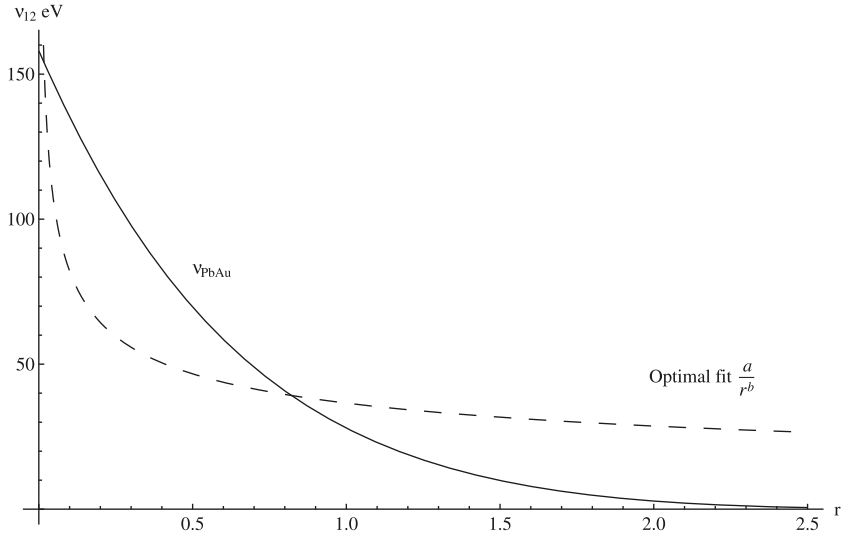

Fig. 3. Au–Au effective two point EAM potential [29, 31] with N_c = 11.7 and inverse power fit.

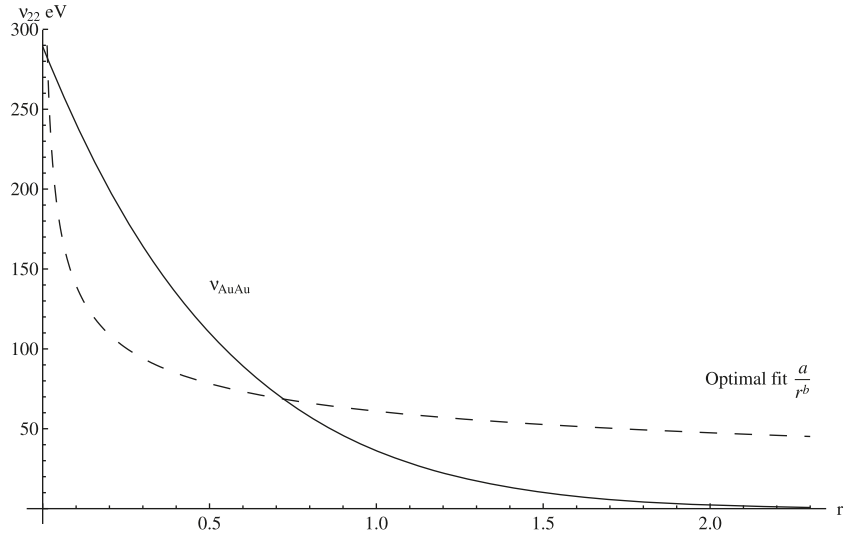

expression for the isothermal susceptibility as a linear function of the temperature can be derived:

$$\chi_{ex}(T) = -0.011043395 + 0.3230992 \times 10^{-4} T$$

There are no units since the static structure factor is nondimensional. For low solute concentrations, this leads to the following expression for the experimental isothermal compressibility of the liquid alloy:

$$\chi_{ex}^{T}(T) = \frac{\chi_{ex}(T)}{\rho(T) k_B T} \tag{7}$$

Development of the rational function approximation for the pRDF [8] provides an approximation for the isothermal compressibility. Briefly, for n = 1, 2, 3, and species radii σ_i, let

$$\xi_n = \rho \sum_{i=1}^{N_s} x_i (2\sigma_i)^n \tag{8}$$

and define the volume packing fraction by

$$\eta = \frac{\pi}{6} \xi_3 \tag{9}$$

Then the isothermal compressibility is given by

$$\chi_c^T(T, \sigma_1, \cdots, \sigma_{N_s}) = \frac{1}{k_B T \left(\frac{\rho}{(1-\eta)^2} + \pi \frac{\xi_1 \xi_2}{(1-\eta)^3} + \frac{\pi^2}{36} \xi_2^3 \frac{9 - 4\eta + \eta^2}{(1-\eta)^4} \right)} \tag{10}$$

Setting (7) equal to (10) gives an additional constraint, the isothermal compressibility constraint, for determining the mean coordination number N_c

$$\chi_c^T(T, \sigma_1, \cdots, \sigma_{N_s}) - \chi_{ex}^T(T) = 0 \tag{11}$$

Since (11) depends of the hard-sphere radii, while (5) depend on N_c, (11) and (5) form a simultaneous system for the radii and mean coordination number N_c.

2.5. Mean coordination number constraint for N_c

For a multispecies liquid, the mean coordination number is often estimated by integrating the partial radial distribution functions [15]. A computed mean coordination number,

denoted by compN$_c$, is defined by

$$\mathrm{compN_c}(T, \sigma_1, \cdots, \sigma_{N_s}, N_c) = 4\pi\rho(T)\sum_{i=1}^{N_s}\sum_{j=1}^{N_s} x_i x_j \times \int_{\sigma_{ij}}^{R_{ij}^{\min}(N_c)} g_{ij}(r) r^2 \, \mathrm{d}r \quad (12)$$

The upper limit of each integral, $R_{ij}^{\min}(N_c)$, is the first minimum of $g_{ij}(r)$ beyond σ_{ij}. The mean coordination number constraint is defined by

$$\mathrm{compN_c}(T, \sigma_1, \cdots, \sigma_{N_s}, N_c) - N_c = 0 \quad (13)$$

2.6. Statement of perturbation model

The perturbation model is now defined as the following:

> **Model 1:** At a given temperature, T, corresponding density, $\rho(T)$, given by (6), and given species number concentrations, x_i, $1 \le i \le N_s$, (5) and (11) or (13) give $N_s + 1$ nonlinear integral equations, which (uniquely) determine the radii of the corresponding hard-sphere reference liquid and the mean coordination number N_c. This completely determines the hard-sphere reference liquid, while taking into account features of the interatomic potentials, through the solution for N_c.

For a binary alloy with low solute concentration, it is reasonable to assume both species have the same hard-sphere radius. This adds the constraint, $\sigma_{11} - \sigma_{22} = 0$, to the optimization. Introducing a scalar Lagrange multiplier, λ, the optimality conditions become

$$e_1 + \lambda = 0$$
$$e_2 - \lambda = 0$$

and taking the sum of these two equations gives the necessary condition

$$e_1 + e_2 = 0 \quad (14)$$

For a low solute concentration two species alloy, for which it is assumed the solvent and solute atoms have the same radius, the perturbation model is defined as follows:

> **Model 2:** At a given temperature, T, corresponding density, $\rho(T)$, and given species number concentrations, x_i, $1 \le i \le N_s$, (15) and (11) or (13) give two nonlinear integral equations, which (uniquely) determine the one radius of the corresponding hard-sphere reference liquid and the mean coordination number N_c.

The mass diffusion coefficients of the liquid of interest are then inferred from the Enskog equation applied to the hard-sphere reference liquid. In particular

$$D_{ij} = \frac{3}{8\rho g_{ij}(\sigma_{ij})\sigma_{ij}^2}\left(\frac{k_B T}{2\pi\mu_{ij}}\right)^{1/2} \quad (15)$$

with species i having mass m_i, species i and j having reduced mass $\mu_{ij} = m_i m_j/(m_i + m_j)$, interspecies diameters $\sigma_{ij} = (\sigma_i + \sigma_j)/2$, with the hard-sphere diameters σ_i given by the solution of (5), and the values of the hard-sphere pRDF $g_{ij}(\sigma_{ij})$ given by the rational function approximation [8] discussed in Subsect. 2.2. A short derivation of the Enskog equation is given in ref. 3.

Fig. 4. Model 1 First step at $T = 602$ K with $\sigma_{11} \neq \sigma_{22}$ and a low value of mean coordination number $N_c \approx 10.18$. Contours of error functions e_1, continuous lines, and e_2, broken lines, are shown. A solution $\sigma_{11} \approx 1.48$ Å and $\sigma_{22} \approx 0.92$ Å is given by the intersection of the $e_1 = 0$ and $e_2 = 0$ contours. The large ranges of σ_{11} and σ_{22} over which one solution has been found suggest there is a relatively small number of isolated solutions.

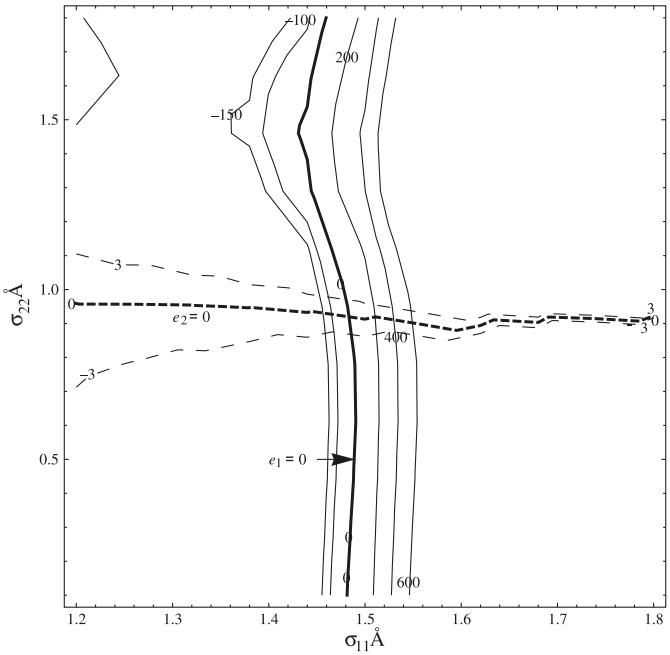

3. Numerical considerations

The partial derivatives in (5) were approximated using central differences with a step size equal to $\sigma_k \times 10^{-2}$. This second-order method was chosen because it requires only two function evaluations, thus reducing CPU demand. The integrals in (5) and (12) were approximated using the simple fourth-order Simpson's rule with at least 160 panels. For the details about both methods see ref. 35. The programs for the RFA approximation of the hard-sphere pRDF [27] are hybrid programs, partially symbolic and partially numerical, written in *Mathematica* [36]. The additional programming for solving the integral equations, constraints for N_c and subsequent estimation of diffusion coefficients required here, was also written in *Mathematica*.

Nonlinear equation solvers produce a series of approximate solutions by an iterative Newton–Raphson-like process until the difference between these is less than a prescribed tolerance or divergence is evident. However, an initial estimate of the solution must always be supplied. Initialization is discussed in the next section.

4. Initialization

For nonlinear systems there is no general procedure for finding an initial solution. Rather some systematic search procedure is required for generating initial solutions. Initialization procedures are described here for **Model 1** and **Model 2**.

Fig. 5. Model 1 Second step at $T = 602$ K by incrementally increasing the mean coordination number N_c by $\Delta N_c = 0.01$. Starting from σ_{11} and σ_{22} given in Fig. 4, equations e_1 and e_2 are solved at each increment, using the previous radii as the initial estimate, after which the isothermal compressibility condition given by (11) is tested. At $N_c \approx 10.88$ the correct isothermal compressibility is satisfied giving a solution of all three equations, referred to as the upper solution, exhibited in Table 1.

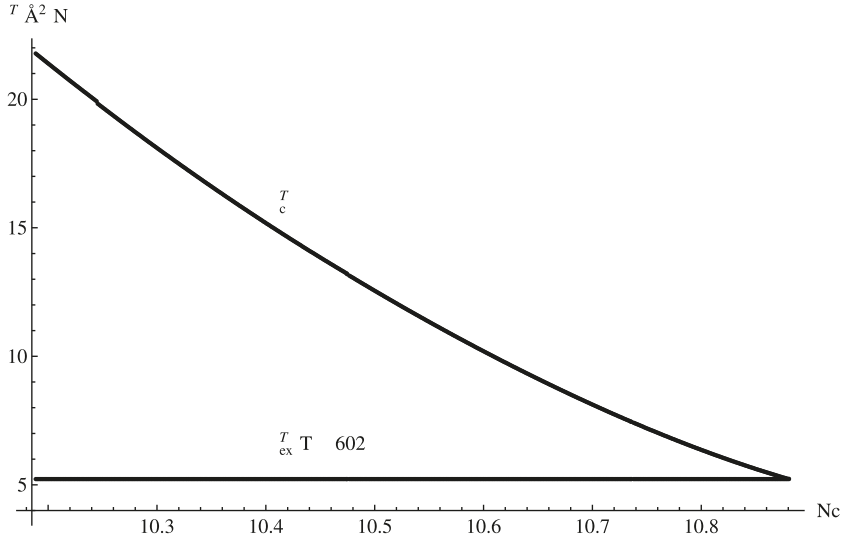

Table 1. Initial solutions.

Model	Name	σ_{11}	σ_{22}	N_c
Model 1	Upper	1.64379	1.16756	10.88010
Model 1	Lower	1.63870	1.74842	11.61010
Model 2	S3	1.63993	1.63993	11.60424
Model 2	S4	1.63993	1.63993	10.92532

4.1. Initialization for Model 1

Initialization was done at a temperature of $T = 602$ K, near the melting temperature T_m, so the ionic radii $r_{Pb} = 1.746$ Å and $r_{Au} = 1.44$ Å would be relevant in determining the range of radii over which to search. But $T = 602$ K is high enough above T_m to avoid any irregularities in the liquid state interatomic potentials that might develop near T_m. Although a full search over all three variables is possible, it always is more manageable to take two at a time.

First step:

Equations e_1 and e_2 defined by (5) were evaluated over a large range of values for σ_1 and σ_2. A constant value of $N_c = 10.18$ was chosen to represent a dense liquid. The results are shown in Fig. 4.

Only one solution of $e_1 = 0$ and $e_2 = 0$ occurs. This is at $\sigma_{11} \approx 1.48$ Å and $\sigma_{22} \approx 0.92$ Å. However, at $N_c = 10.18$ these two radii do not necessarily solve (11).

Second step:

N_c is increased incrementally by $\Delta N_c = 0.01$ with the equations $e_1 = 0$ and $e_2 = 0$ resolved at each increment using the previous values of σ_{11} and σ_{22} as initial estimates. This is shown in Fig. 5. At $N_c \approx 10.88$ the isothermal compressibility has decreased until it equals the experimental value and (11) is satisfied. The resulting initial solution, the upper initial solution, is shown in Table 1.

Preliminary calculations suggest a second initial solution might exist at high mean coordination numbers. Starting from the upper initial solution, N_c was again increased incrementally. The results are shown in Fig. 6. Initially the isothermal compressibility decreases, but after reaching a minimum, it increases and finally satisfies (11) at $N_c \approx 11.6$. This determines a second initial solution, the initial lower solution shown in Table 1. Since the isothermal compressibility continues to increase until N_c reaches the fcc crystal limit of $N_c = 12$, no additional solutions are indicated.

4.2. Initialization for Model 2

For **Model 2** the solvent and solute radii are equal. Only two equations (15) and (11) must be evaluated over suitable ranges of the one radius σ_{11}, and mean coordination number N_c. The results are shown in Fig. 7.

Only two possible solutions are indicated at S3 and S4 in the Fig. 7. The S3 and S4 subregions are shown in more detail in Figs. 8 and 9. Both Figs. 8 and 9 show well-defined unique solutions with contours intersecting with different tangent lines. The two initial solutions, the initial S3 solution, and initial S4 solution are shown in Table 1.

For both **Model 1** and **Model 2** two initial solutions have been found. The extension of each of these solutions is considered in the next section.

5. Extension of solutions through experimental temperature range

For **Model 1,** two initial solutions referred to as the upper and lower initial solution, have been found. These two solutions are extended across the experimental temperature range by increasing, incrementally, the temperature usually with an increment $\Delta T = 1$ K. At each increment, the three unknowns ($\sigma_{11}(T + \Delta T)$, σ_{22} $(T + \Delta T)$, and N_c $(T + \Delta T)$) are found by simultaneously solving (5) and (11) using the most recent solutions ($\sigma_{11}(T)$, σ_{22} (T), and N_c (T)) as the initial estimate.

For **Model 2**, two initial solutions, the initial S3 and initial S4 solutions, have been found. These two solutions are also extended across the experimental temperature range by

Fig. 6. Model 1 at T = 602 K by incrementally increasing N_c as described in Fig. 5, starting from the upper solution. At $N_c \approx 11.6$ the correct isothermal compressibility is satisfied again giving a second solution, the lower solution, exhibited in Table 1.

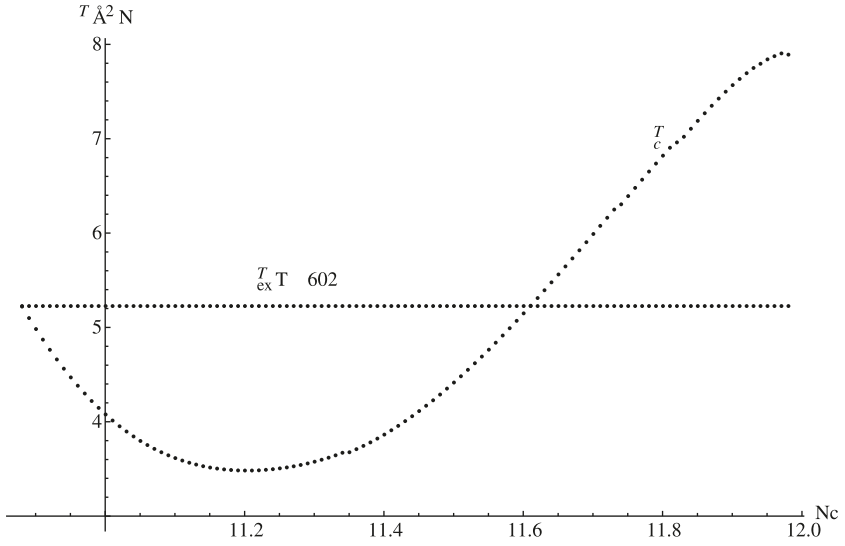

Fig. 7. Model 2 initial search at T = 602 K with $\sigma_{11} = \sigma_{22}$. Contours of error function $e_1 + e_2$, continuous lines, and $\chi^T_{ex} - \chi^T_c$, broken lines, are shown. Two possible solutions are indicated at S3 and S4 at the intersection of the $e_1 + e_2 = 0$ and $\chi^T_{ex} - \chi^T_c = 0$ contours. The large ranges of σ_{11} and N_c over which two possible solutions have been found suggest there are a relatively small number of isolated solutions.

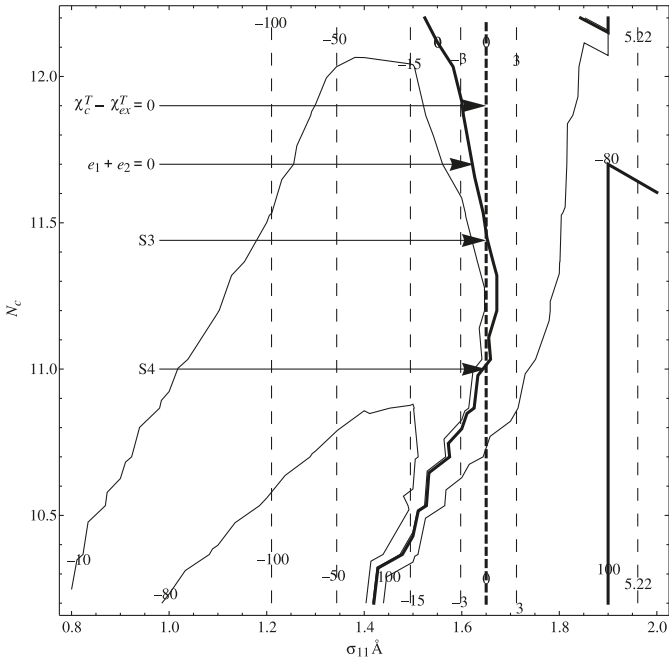

Fig. 8. Model 2 initial search at T = 602 K with $\sigma_{11} = \sigma_{22}$ near S3 in Fig. 7. A solution, the initial S3 solution, is indicated at $\sigma_{11} \approx$ 1.6398 Å and $N_c \approx 11.604$, by intersection of contours at positive angles. The solution is exhibited in Table 1.

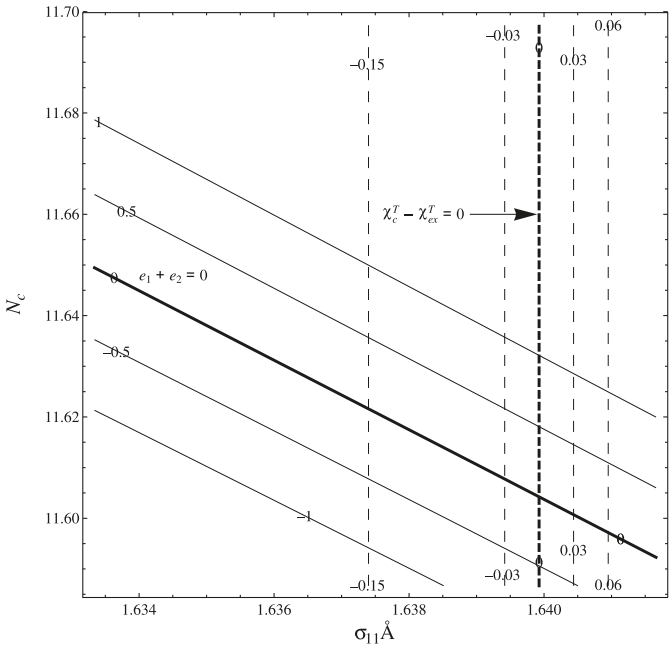

incrementally increasing the temperature. At each increment the two unknowns ($\sigma_{11}(T + \Delta T)$ and N_c $(T + \Delta T)$) are found by simultaneously solving (14) and (11) or (13) using the most recent solutions ($\sigma_{11}(T)$, and N_c (T)) as the initial estimate. For the S3 solution (13) was used in place of (11) at higher temperatures.

For both **Model 1** and **Model 2** the inverse function theorem provides conditions for uniqueness of the extension. An accuracy goal of four was used. This means the first four digits of calculations of the radii and mean coordination number are signifigant. This is reasonable since the radii are in Ångströms and the mean coordination number is usually thought of as an integer. An accuracy goal of four resulted in convergence in under 20 iterations. However, convergence was never achieved with a higher accuracy goal. This probably originates with the second-order approximation of the partial derivatives in (5) and in practise may limit the use of **Model 1** to a small number of species unless symbolic partial derivatives are available.

Fig. 9. Model 2 initial search at $T = 602$ K with $\sigma_{11} = \sigma_{22}$ near S4 in Fig. 7. A solution, the initial S4 solution, is indicated at $\sigma_{11} \approx 1.6398$ Å and $N_c \approx 10.925$, by intersection of contours at positive angles. The solution is exhibited in Table 1.

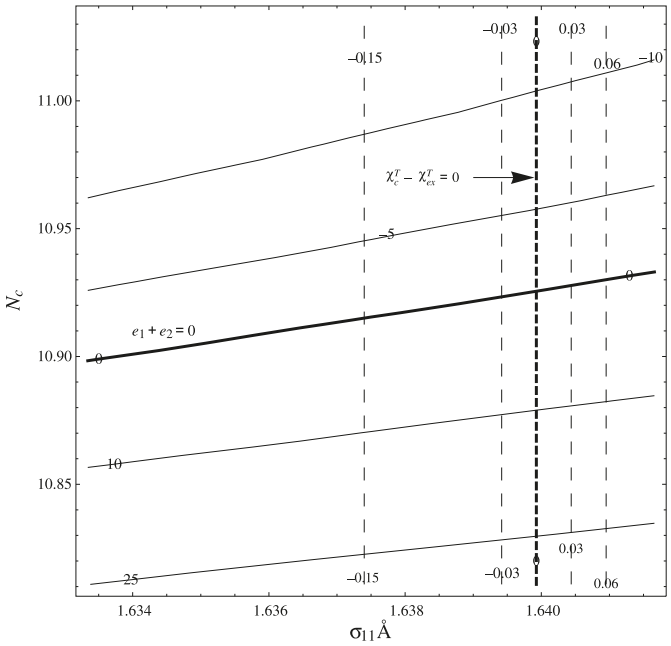

Fig. 10. Pb solvent hard-sphere radius, σ_{11}, in éngstroms, of all four solutions versus temperature T K. The lower solution ends abruptly at $T \approx 790$ K, with a marked change in slope. The equal radii solutions S3 and S4 are essentially identical until S3 ends abruptly at $T \approx 910$ K, which is seen more clearly in Fig. 12. The S3 solution has been extended beyond $T \approx 890$ K, where $N_c = compN_c$ using (13). Notice the mean coordination number criteria is qualitatively quite different from the other solutions and remains almost constant. Also the radius values at $T = 602$ K of all the solutions, including the upper solution, are consistent with the radial distribution function nearest peak distance for liquid Pb near the melting temperature $d_{Pb} = 3.39$ Å, listed in Table 2 of Protopapas et al. [37].

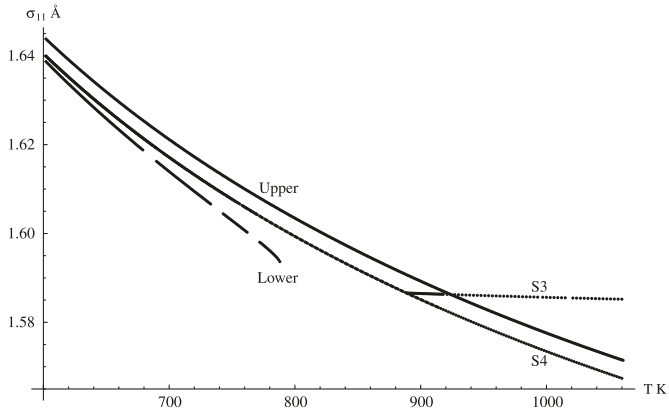

Fig. 11. Au solute hard-sphere radius, σ_{22}, in éngstroms of the lower and upper solutions versus temperature T K. The lower solution ends abruptly at $T \approx 790$ K, with an almost infinite slope, and throughout σ_{22} is greater than the Au ionic radius 1.44 Å. However, for the upper solution, σ_{22} remains less than the Au ionic radius 1.44 Å.

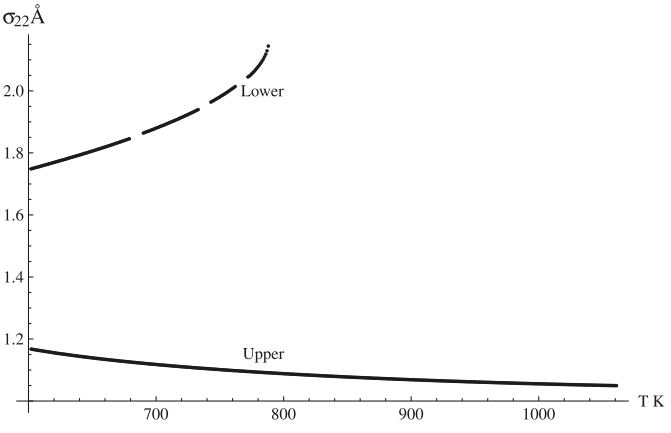

Fig. 12. Mean coordination number N_c of all solutions versus temperature T K. The pairing of the upper solution with the equal radius S4 solution and the lower solution with S3 is evident. It is clear that the S3 solution ended abruptly at $T \approx 910$ K where $N_c \approx 12$, which denotes solid fcc crystal, at which point the liquid isothermal compressibility criterion cannot be satisfied. The extension of S3 using (13) remains almost constant.

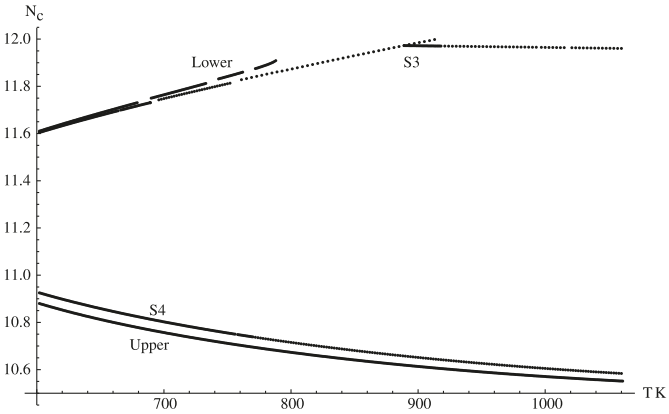

6. Solutions for Model 1 and Model 2

For **Model 1** at temperature T a solution (σ_1, σ_2, N_c) consists of the hard-sphere reference solvent and solute radii and mean coordinate number. Two initial solutions for **Model 1**, the upper and lower initial solutions, were found in Subsect. 4.1. For **Model 2** at temperature T a solution (σ_1, N_c) consists of the hard-sphere reference solvent and solute radius and mean coordinate number. Two initial solutions for **Model 2**, the S3 and S4 initial solutions, were found in Subsect. 4.2. The method for extending both model solutions was described in Subsect. 5. The resulting solutions are shown in Figs. 10–12 as functions of temperature over the temperature range of experimental data in Smith [1].

For all four solutions the Pb hard-sphere solvent radius, σ_{11}, at = 602 K is consistent with the radial distribution function nearest peak distance for liquid Pb near the melting temperature, $d_{Pb} = 3.39$ Å, listed in Table 2 of Protopapas et al. [37], and always less than the Pb ionic radius $r_{Pb} = 1.746$ Å. The S3 and S4 solutions are essentially identical until the S3 solution ends abruptly. The S3 solution was extended using (13) in place of (11) and, from Figs. 10 and 12, it is clear the mean coordination number constraint gives a nearly constant solution.

Fig. 13. Schematic of Pb 1 wt % Au capillary diffusion apparatus. Initial pure Pb solvent plug and Pb 1 wt % Au solute plug.

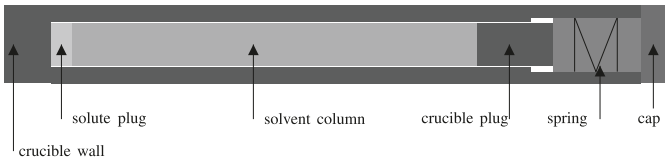

Figure 11 shows that the Au hard-sphere solute radius, σ_{22}, remains below the Au ionic radius r_{Au} = 1.44 Å for the upper solution, but remains above this value for the lower solution. Also the lower solution ends abruptly at $T \approx 790$ K, with an almost infinite slope.

Figure 12 shows the natural pairing of the upper solution with S4 and the lower solution with S3. Both the upper solution and S4 represent liquids with lower mean coordination number N_c. The lower solution and S3 represent a transition to a glassy solid with high mean coordination number near to that of the fcc crystal value of $N_c = 12$. This is inconsistent with the experimental isothermal compressibility data for liquid Pb. For the lower solution, satisfying (11) leads to an almost infinite rate of increase of σ_{22} at $T \approx 790$ K. For S3 an abrupt stop occurring at $T \approx 910$ K where $N_c \approx 12$.

Several properties of the liquid of interest, in this case Pb 1 wt % Au could be inferred from these solutions for a hard-sphere reference liquid. This includes an approximate equation of state and all thermodynamic variables that can be determined from partial derivatives of the equation of state. However, for this study, the practical application was to determine the mass diffusion coefficients by use of the Enskog eq. (15) and make comparisons with the experimental results in Smith et al. [1]. This is done in the next section.

7. Inferred mass diffusion coefficients and comparison with experimental results

High-quality experimental observations of the mass diffusion coefficient for the Pb 1 wt % Au liquid alloy performed in microgravity with additional isolation from "*g*-jitter" are available in ref. 1 by Smith. In this section, the mass diffusion coefficients inferred from **Model 1** and **Model 2** by applying (15) are compared with these experimental observations.

First the capillary mass diffusion apparatus is indicated schematically in Fig. 13. An initial Au gradient exists between the solute plug and the solvent column resulting in Au diffusion into the solvent column. However, an initial Pb gradient also exists between the solvent column and the solute plug resulting in a reverse Kirkaldy effect [38], generating diffusion of Pb into the solvent plug. To describe the simultaneous diffusion of both species a total diffusion coefficient D_{tot} was introduced in ref. 3. Although not used here in any calculations, the Green–Kubo [15] velocity correlation expression for mass diffusion coefficients is most instructive for motivating the definition of D_{tot}. Weighing the species velocity by the species concentrations gives a mixed velocity field $v(t) = \sum_{i=1}^{N_s} x_i v_i(t)$. Applying the Green–Kubo elation to the mixed velocity field gives the following expression for the total diffusion D_{tot}:

$$D_{\text{tot}} = \frac{1}{3}\int_0^\infty \left\langle \sum_{i=1}^{N_s} x_i v_i(t) \cdot \sum_{j=1}^{N_s} x_j v_j(0) \right\rangle \mathrm{d}t = \sum_{i=1}^{N_s} x_i^2 D_{ii} \qquad (16)$$

Diffusion coefficients versus temperature computed using (15) are shown for the lower solution and S3 solution in Fig. 14. The large values of σ_{22} given by the lower solution result in low values of D_{12}^{L} and D_{22}^{L}. Also, D_{22}^{L} decreases with temperature, which suggests inconsistency between a transition into a glassy solid at high coordination numbers and use of the isothermal compressibility constraint with experimental data for liquid Pb. D_{11}^{L} and D_{tot}^{L} computed using (16) are almost identical to MB a solution assuming equal solvent and solute radii and satisfying the isothermal compressibility constraint described by Scott et al. [3]. This indicates that the isothermal compressibility constraint is very important. D^{S3} is also almost identical to the MB solution except where S3 was solved using the mean coordination number constraint, where D^{S3} is lower, indicating the mean coordination number constraint is not suitable and emphasizing the importance of the isothermal compressibility constraint. D_{11}^{L}, D_{tot}^{L}, D^{S3}, and MB make good agreement with the experimental data of Smith [1] indicating the capillary experimental essentially measures D_{tot}.

Diffusion coefficients versus temperature are shown for the upper solution and S4 solution in Fig. 15. The smaller values of σ_{22} given by the upper solution result in high values of D_{12}^{U} and D_{22}^{U}. Also, D_{12}^{U} is in reasonable agreement with the velocity correlation estimate of the mixed diffusion coefficient obtained from the molecular dynamic simulations, (MD), of Scott et al. [2]. D_{11}^{U}, D_{tot}^{U}, and D^{S3} are almost identical to MB in Scott et al. [3], again indicating the importance of the isothermal compressibility constraint. D_{11}^{U}, D_{tot}^{U}, D^{S4}, and MB make good agreement with the experimental data of Smith [1].

The description of initialization in Sect. 4 and Figs. 4–9 therein as well as the description of the extension process in Sect. 5 indicate that the solutions used here have not been forced or manipulated. The close agreement between D_{12}^{U} and "MD" from [2], and the close agreement between D_{tot}^{U} and D_{11}^{U} and the experimental results of Smith [1] are a consequence of the properties of the optimality criteria (5), effective embedded atom-like glue potentials described in Subsect. 2.3, the isothermal compressibility constraint described in Subsect. 2.4, and the rational function approximation of the hard-sphere pRDF described in Subsect. 2.2. Some of the loss of agreement with increasing temperature may result from the low-accuracy goal required for convergence. This might be avoided by extending the solutions from initializations made at several intermediate temperatures.

8. Conclusions

Two numerical models **Model 1** and **Model 2** limited to a binary liquid have been developed for describing dilute N_s-species liquids. The models are based on perturbation theory in which a minimum of an upper bound on the difference in internal energy between the liquid of interest and a reference hard-sphere liquid is sought. The Lado minimization criteria [20, 22] is applied. To provide the pRDF of the reference hard-sphere alloy, the recent and effective rational function

Fig. 14. Diffusion coefficients versus temperature. Experimental data, circles, and linear fit, Smith [1]. Mass diffusion coefficients D^{L}_{11}, D^{L}_{12}, and D^{L}_{22} of lower solution, extrapolated linearly above $T = 790$ K as broken lines. D^{L}_{tot} is computed using (16). D^{S3} of equal radius solution S3, broken white line, and broken line above $T \approx 910$ K. MB, thick broken line, from Scott et al. [3]. Note that D^{L}_{22} decreases with temperature. Note that MB, D^{L}_{11}, D^{L}_{tot}, and D^{S3} are almost identical and make good agreement with the experimental data especially at low temperatures.

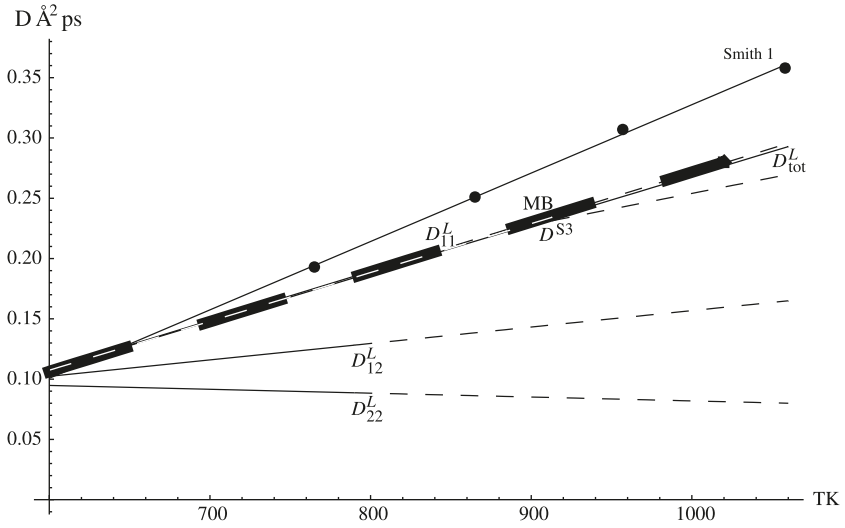

Fig. 15. Diffusion coefficients versus temperature. Experimental data, circles, and linear fit, Smith [1]. Mass diffusion coefficients D^{U}_{11}, D^{U}_{12}, and D^{U}_{22} of upper solution. D^{U}_{tot} computed using (16). D^{S4} of equal radius solution *S*4. MD and linear fit, long broken line, from Scott et al. [2]. MB, thick broken line, from Scott et al. [3]. Note that MB, D^{U}_{11}, D^{U}_{tot}, and D^{S4} are almost identical and make good agreement between the experimental data especially at low temperatures. Also note the good agreement between MD and D^{U}_{12}.

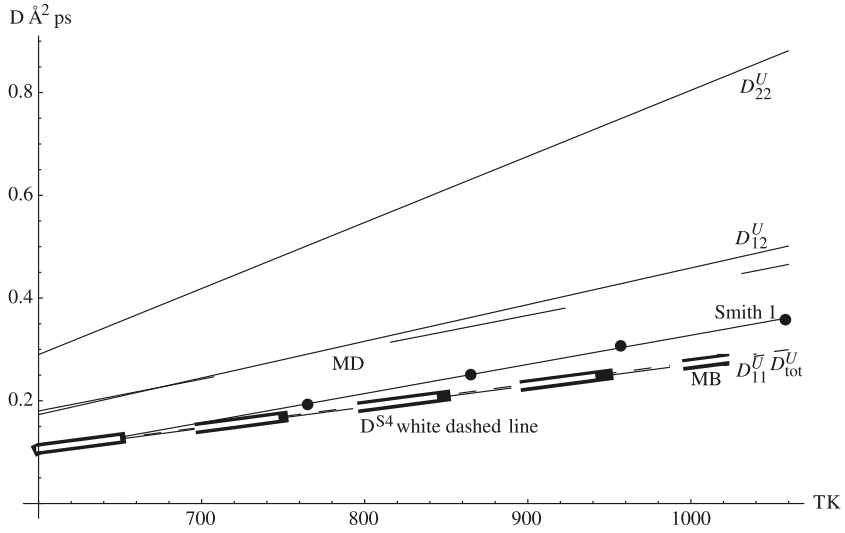

approximation developed by Yuste et al. [7, 8] has been used. To describe the liquid of interest a two-point effective potential based on the embedded atom-like glue potential of Ercolessi et al. [28, 29] has been used. An additional parameter, the mean coordination number, is required to completely specify the effective two-point potential. The mean coordination number was determined by adding one of two possible constraints to the optimization procedure. Setting the isothermal compressibility approximation given by the rational function approximation equal to available experimental values of the isothermal compressibility gave one constraint, the isothermal compressibility constraint. Setting the mean coordination number equal to the coordination number computed using the partial radial distribution functions gave a second constraint, the mean coordination number constraint. Numerical solutions were obtained for a Pb 1 wt % Au liquid. The initialization process indicating two solutions, one at low mean coordination number, $N_c < 11$, and one at a high mean coordination number, $N_c > 11.6$, for both models was described and demonstrated as well as the process to extend the solutions to higher temperatures. The following remarks characterize the solutions.

Initial solutions having $N_c > 11.6$ tended to stop at lower temperatures as the solute radius grows very quickly or N_c reaches the fcc crystal value of $N_c = 12$. With N_c so high, these solutions represent transition from a liquid to a glassy solid and develop an inconsistency with the isothermal compressibility constraint that uses experimental data for liquid Pb.

The initial solutions with $N_c < 11$ have been extended across the temperature range of the experimental data of Smith [1]. In all cases the hard-sphere solvent radius at T = 602 K is consistent with the radial distribution function nearest peak distance for liquid Pb near the melting temperature d_{Pb} = 3.39 Å, listed in Table 2 of Protopapas et al. [37].

Although only the one binary liquid has been considered it is believed the models will apply to other binary liquids, and at higher solute concentrations when the isothermal compressibility of the binary liquid is known, and to a higher number of species if certain limitations in estimating partial derivatives in the minimality criteria can be overcome. The models have been used to estimate the mass diffusion coefficients of Pb 1 wt % Au liquid by applying the Enskog equation to the reference hard-sphere liquid.

The estimates have been compared with the experimental observations of Smith [1]. To aid in the comparison, a total mass diffusion coefficient D_{tot} has been defined for application in situations were reverse Kirkaldy effect simultaneous diffusion may be in effect.

The almost identical values of MB from ref. 3, with D_{11}^{L}, D_{tot}^{L}, D^{S3}, D_{11}^{U}, D_{tot}^{U}, and D^{S4} show the importance of the isothermal compressibility constraint. This is further indicated by the lower values of D^{S3} when the alternative mean coordination number constraint is used. The importance of the isothermal compressibility constraint is perhaps obvious because the mass diffusion coefficients can be determined from the structure factor (Chapt. 22 in ref. 5). The close agreement of these estimates with the experimental data of Smith [1], indicate that the reverse Kirkaldy effect (simultaneous diffusion) has been influential. This conclusion was also reached in ref. 3.

The close agreement between D_{12}^{U} and the the velocity correlation estimate of the mixed diffusion coefficient obtained from molecular dynamic simulations of Scott et al. [2] indicate that a good estimate of the mixed diffusion coefficient can be achieved using **Model 1**. However, in the case of capillary experiments, this can be tested only indirectly through comparison of D_{tot} with the experimental data.

Model 1 and **Model 2** may assist in the analysis of data from both Earth-bound and microgravity mass diffusion experiments.

Acknowledgements

The authors gratefully acknowledge support through funding from the National Science and Engineering Research Council of Canada (NSERC).

References

1. R.W. Smith. Microgravity Sci. Technol. **XI**, 78 (1998).
2. P.J. Scott and R.W. Smith. J. Appl. Phys. **104**, 043706 (2008). doi:10.1063/1.2969663.
3. P.J. Scott and R.W. Smith. J. Phys. Condens. Matter, **21**, 335104 (2009). doi:10.1088/0953-8984/21/33/335104.
4. S. Chapman and T.G. Cowling. The mathematical theorey of non-uniform gases. Cambridge University Press, Cambridge, UK. 1939.
5. D.A. McQuarrie. Statistical mechanics. University Science Books, Sausalito. 2000.
6. P.J. Scott and R.W. Smith. Manuscript in preparation.
7. S.B. Yuste and A. Santos. Phys. Rev. A, **43**, 5418 (1991). doi:10.1103/PhysRevA.43.5418. PMID:9904854.
8. S.B. Yuste, A. Santos, and M. López de Haro. J. Chem. Phys. **108**, 3683 (1998). doi:10.1063/1.475762.
9. M.S. Daw and M.I. Baskes. Phys. Rev. Lett. **50**, 1285 (1983). doi:10.1103/PhysRevLett.50.1285.
10. M.S. Daw and M.I. Baskes. Phys. Rev. B, **29**, 6443 (1984). doi:10.1103/PhysRevB.29.6443.
11. S. Dalgiç and M. Çolakoğullari. Turk. J. Phys. **30**, 303 (2006).
12. A.Z. Ziauddin Ahmed and G.M. Bhutyan. Int. J. Mod. Phys. B, **16**, 3837 (2002). doi:10.1142/S0217979202013171.
13. C. Dariva, L.A.F. Coelho, and J.V. Oliveira. Ciènc.Tecnol. Aliment. **17**, 461 (1997).
14. R.W. Zwanzig. J. Chem. Phys. **22**, 1420 (1954). doi:10.1063/1.1740409.
15. J.-P. Hansen and I.R. McDonald. Theory of simple liquids. Academic Press, Boston. 2006.
16. G.A. Mansoori and F.B. Canfield. J. Chem. Phys. **51**, 4958 (1969). doi:10.1063/1.1671889.
17. A.H. Alem and G.A. Mansoori. Am. Inst. Chem. Eng. J. **30**, 468 (1984). doi:10.1002/aic.690300316.
18. K.K. Mon. Phys. Rev. E Stat. Nonlin. Soft Matter Phys. **63**, 061203 (2001). PMID:11415076.
19. D. Ben-Amotz and G. Stell. J. Chem. Phys. **120**, 4844 (2004). doi:10.1063/1.1647520. PMID:15267344.
20. F. Lado. Mol. Phys. **52**, 871 (1984). doi:10.1080/00268978400101621.
21. H.C. Andersen, J.D. Weeks, and D. Chandler. Phys. Rev. A, **4**, 1597 (1971). doi:10.1103/PhysRevA.4.1597.
22. E. Enciso, F. Lado, M. Lombardero, J.L.F. Abascal, and S. Lago. J. Chem. Phys. **87**, 2249 (1987). doi:10.1063/1.453153.
23. H. Reiss, H.L. Frisch, and J.L. Lebowitz. J. Chem. Phys. **31**, 369 (1959). doi:10.1063/1.1730361.
24. J.L. Lebowitz. Phys. Rev. **133**, 4A, A895 (1964). doi:10.1103/PhysRev.133.A895.
25. A. Malijevský, A. Malijevský, S.B. Yuste, A. Santos, and M. López de Haro. Phys. Rev. E Stat. Nonlin. Soft Matter Phys. **66**, 061203 (2002). PMID:12513273.
26. A. Trokhymchuk, I. Nezbeda, J. Jirsák, and D. Henderson. J. Chem. Phys. **123**, 024501 (2005). doi:10.1063/1.1979488.
27. http://www.unex.es/fisteor/santos/sby.html.
28. H.S. Lim, C.K. Ong, and F. Ercolessi. Surf. Sci. **269-270**, 1109 (1992). doi:10.1016/0039-6028(92)91401-V.
29. F. Ercolessi, M. Parrinello, and E. Tosatti. Philos. Mag. A, **58**, 213 (1988). doi:10.1080/01418618808205184.
30. A. Landa, P. Wynblatt, D.J. Siegel, J.B. Adams, O.N. Mryasov, and X.-Y. Liu. Acta Mater. **48**, 1753 (2000). doi:10.1016/S1359-6454(00)00002-1.
31. S.M. Foiles. Phys. Rev. B, **32**, 3409 (1985). doi:10.1103/PhysRevB.32.3409.
32. A.E. Schwaneke and W.L. Falke. J. Chem. Eng. Data, **17**, 291 (1972). doi:10.1021/je60054a016.
33. M. Stojić, B. Babić Stojić, and D. Milivojević. Physica B, **334**, 274 (2003). doi:10.1016/S0921-4526(03)00077-2.
34. S.I. Filippov, N.B. Kazakov, and L.A. Pronin. Chern. Metallurg. **9**, 8d (1966).
35. R.L. Burden and J. Douglas Faires. Numerical analysis. Prindel, Weber and Schmidt, Boston. 1985.
36. Wolfram Research Inc. *Mathematica* Version 6.0.3, Champagne, Ill. USA. 2008.
37. P. Protopapas, H.C. Andersen, and N.A.D. Parlee. J. Chem. Phys. **59**, 15 (1973). doi:10.1063/1.1679784.
38. J.S. Kirkaldy and D.J. Young. Diffision in the condensed state. The Institute of Metals, London. 1987.